

# Comprehensive assessment of miniature CRISPR-Cas12f nucleases for gene disruption

Received: 6 June 2022

Accepted: 14 September 2022

Published online: 24 September 2022


 Check for updatesChangchang Xin<sup>1,2</sup>, Jianhang Yin<sup>1,2</sup>, Shaopeng Yuan<sup>1</sup>, Liqiong Ou<sup>1</sup>, Mengzhu Liu<sup>1</sup>, Weiwei Zhang<sup>1</sup> & Jiazhi Hu<sup>1</sup>  

Because of their small size, the recently developed CRISPR-Cas12f nucleases can be effectively packaged into adeno-associated viruses for gene therapy. However, a systematic evaluation of the editing outcomes of CRISPR-Cas12f is lacking. In this study, we apply a high-throughput sequencing method to comprehensively assess the editing efficiency, specificity, and safety of four Cas12f proteins in parallel with that of Cas9 and two Cas12a proteins at multiple genomic sites. Cas12f nucleases achieve robust cleavage at most of the tested sites and mainly produce deletional fragments. In contrast, Cas9 and Cas12a show relatively higher editing efficiency at the vast majority of the tested sites. However, the off-target hotspots identified in the Cas9- and Cas12a-edited cells are negligibly detected in the Cas12f-edited cells. Moreover, compared to Cas9 and Cas12a nucleases, Cas12f nucleases reduce the levels of chromosomal translocations, large deletions, and integrated vectors by 2- to 3-fold. Therefore, our findings confirm the editing capacity of Cas12f and reveal the ability of this nuclease family to preserve genome integrity during genome editing.

The clustered regularly interspaced short palindromic repeats (CRISPR)-CRISPR-associated protein (Cas) system in bacteria has been engineered into a robust genome-editing tool that can be used to manipulate the mammalian genome efficiently. The earliest Cas protein to be applied to mammalian gene editing was *Streptococcus pyogenes* Cas9 (*SpCas9*) in the type II CRISPR-Cas system<sup>1,2</sup>. Then, type V-A Cas12a, which mainly includes *Acidaminococcus* sp. Cas12a (*AsCas12a*) and *Lachnospiraceae bacterium* Cas12a (*LbCas12a*), was demonstrated to be powerful for gene modulation<sup>3-5</sup>. Cas9 and Cas12a are the most prevalent gene-editing tools and show great potential for clinical use<sup>6-11</sup>. However, because they are large, neither of these proteins can be efficiently packaged into a single adeno-associated viral (AAV) particle, limiting the broad application of Cas9 and Cas12a systems in vivo<sup>12-14</sup>. Hence, new miniature CRISPR-Cas systems have been recently developed to accommodate the payload size (<4.7 kb) needed for AAV delivery<sup>15,16</sup>. For example, the Class II type V-E nuclease *Planctomyces* Cas12e (*PlmCas12e*, also known as *PlmCasX*), a 978-amino acid (aa) protein, has been reported to functionally edit the human genome<sup>17-19</sup>.

Moreover, the most recently reported Class II type V-F Cas12f proteins, including *UnICas12f1* from an uncultured archaeon and previously named Cas14a<sup>20-22</sup>, CasMINI (a protein engineered from *UnICas12f1*), and *Acidibacillus sulfuroxidans* Cas12f1 (*AsCas12f1*), consisting of 529 aa, 529 aa, and 422 aa, respectively, have shown robust mammalian cell-editing activity maintaining a small protein size<sup>23,24</sup>.

Cas12e recognizes a 5'-TTCN protospacer adjacent motif (PAM) and generates two broken sticky ends by predominantly cleaving DNA at two distinct positions -10 nucleotides (nt) apart in a nontarget strand (NTS) and target strand (TS)<sup>17</sup>. This cleavage pattern is similar to that of Cas12a but different from that of Cas9. *UnICas12f1* cleaves double-stranded DNA with a 5'-TTTR PAM and introduces DNA breaks in a staggered cutting pattern, and the overhang can be as long as 10 base pairs (bp)<sup>22</sup>. *AsCas12f1* has been shown to predominantly cleave DNA at the 3rd nt downstream of a spacer in the TS and simultaneously generate two breaks in the NTS, with one located at the 12th nt and the other located at approximately the 23rd-27th nt downstream of a PAM, producing 5'-overhangs of -11-bp<sup>24</sup>. The emergence of these

<sup>1</sup>The MOE Key Laboratory of Cell Proliferation and Differentiation, Genome Editing Research Center, School of Life Sciences, Peking-Tsinghua Center for Life Sciences, Peking University, 100871 Beijing, China. <sup>2</sup>These authors contributed equally: Changchang Xin, Jianhang Yin.  e-mail: [hujz@pku.edu.cn](mailto:hujz@pku.edu.cn)

miniature CRISPR-Cas toolboxes has broadened the target range for editing the human genome and provides a convenient choice for gene delivery in the clinic.

However, in addition to inducing gene disruptions at a target site, CRISPR-Cas can cause unintended off-target cleavage at imperfectly matched loci<sup>25–28</sup>. Moreover, it can lead to unwanted structural variations in the chromosome, including chromosomal translocations, large deletions, and integration of exogenous DNA<sup>29–36</sup>. These byproducts severely threaten genome integrity and are associated with oncogenesis, raising great concern over the safety of genome editing. Comprehensive assessments of these newly developed miniature Cas12 nucleases on the specificity and genomic structural variations generated during genome editing are lacking, which has restricted the further optimization of miniature Cas enzyme-guided strategies in clinical gene-editing applications<sup>37</sup>.

In this study, we assess the activity and safety of the above-mentioned Cas nucleases in depth. Here, we present a full spectrum of editing outcomes, including off-target mutations and structural variations, induced by Cas12f, which are evaluated in parallel with Cas9 and Cas12a. We conclude that Cas12f can induce efficient cleavage at some genomic sites with fewer off-target cleavage events and structural variations. Among the Cas12f types tested, CasMINI shows the most consistent editing ability and specificity at most of the tested genomic sites.

## Results

### Assessment of the editing ability of Cas12f nucleases as determined by EGFP silencing assay

To compare the editing ability of various CRISPR-Cas12 nucleases, we constructed a destabilized-enhanced green fluorescent protein (EGFP)

reporter system by integrating the EGFP gene into the *AAVS1* safe harbor locus in HEK293T cells (Fig. 1a). We then cloned *Un1Cas12f1*, CasMINI, *AsCas12f1*, and *PlmCas12e* as well as *SpCas9*, *AsCas12a*, and *LbCas12a* into the same plasmid backbone and coexpressed these plasmids with a puromycin resistance gene fused via a P2A self-cleavage peptide (Fig. 1b, c). Notably, optimized single guide (sg) RNA version 4.1 was used for *Un1Cas12f1* because it had been previously reported to show effective editing<sup>20</sup>. We also introduced this engineered sgRNA *ge4.1* into CasMINI to generate CasMINI *ge4.1*. To test the editing efficiency, we designed two target sites for each CRISPR-Cas nuclease (Supplementary Fig. 1a), in which the gRNAs recognized the EGFP locus at similar loci but with offsets to satisfy differences in PAM specificity (Fig. 1b). The cells were selected with puromycin for 3 days and then assayed for GFP disruption by flow cytometry 5 and 10 days post-transfection (Fig. 1c). We used the proportion of GFP-negative cells to estimate the gene disruption rates of each nuclease, although the former may have been lower than the latter measure (Supplementary Fig. 1b, c).

Complete degradation of GFP requires a long time, and we indeed detected an obvious increase in the GFP-negative cell population 10 days post-edit compared to that observed 5 days post-edit (Supplementary Fig. 1b). Then, we used the proportion of GFP-negative cells measured 10 days post-transfection to make a final assessment. All the tested editing nucleases induced varying degrees of gene expression disruption, with Cas9 and two Cas12a enzymes exhibiting the highest editing efficiency at both target sites (>42.5%) (Fig. 1d and Supplementary Table 1). *Un1Cas12f1* *ge4.1* and CasMINI *ge4.1* showed relatively lower but useful levels of editing efficiency at the two target sites, ranging from 18.3 to 26.2%. Notably, CasMINI exhibited a high efficiency at

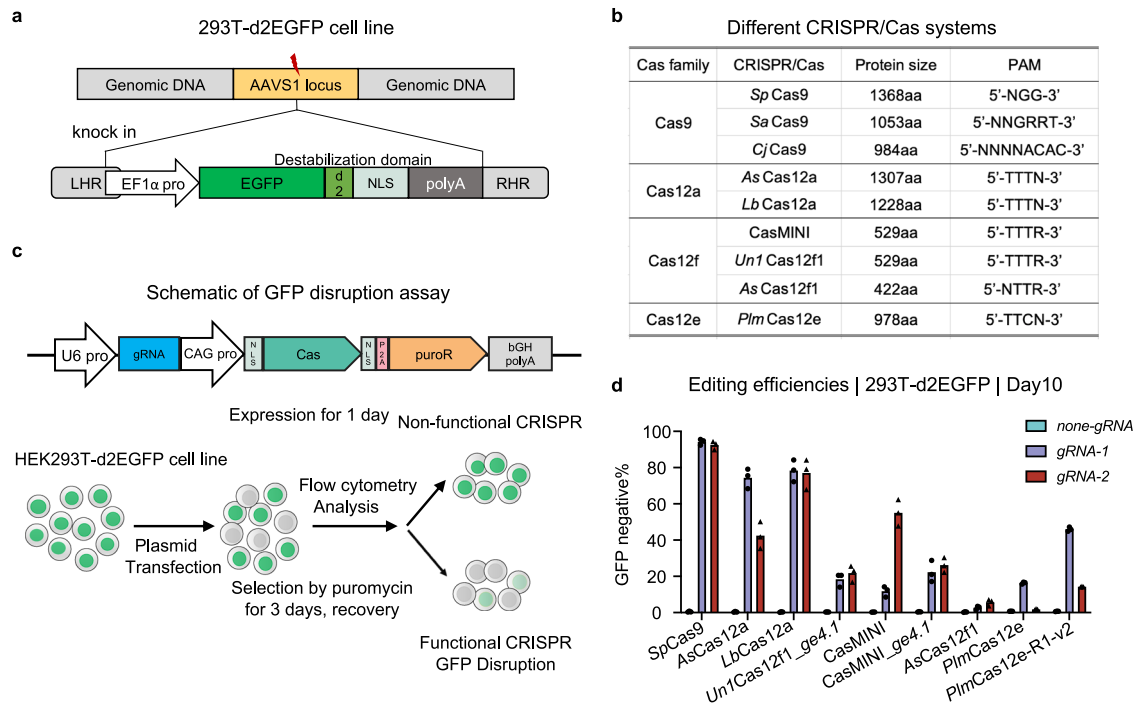


### Fig. 1 | Cas12f nucleases efficiently disrupted EGFP gene expression in vivo.

**a** Schematics showing the 293T-d2EGFP cell lines. Lightning represents the position of *SpCas9*-induced double-strand break (DSB). A gene target plasmid to cut the *AAVS1* site and an integration donor plasmid are used to achieve the site-specific exogenous d2EGFP gene insertion. LHR and RHR represent left or right homo-arm, respectively. “pro” represents promoter. **b** Summary of different CRISPR-Cas systems. **c** Schematic showing the editing efficiency detection assay with the HEK293T-d2EGFP cell lines. “pro” represents promoter. “puroR” represents the puromycin resistance gene. “NLS”

represents nuclear localization sequence. The plasmids carrying Cas nuclease and single guide (sg) RNA that could target the EGFP gene are transfected to d2EGFP cells. After the protein is expressed 1 day, add puromycin to select the positive transfection cells and do the flow cytometry analysis. **d** The GFP disruption efficiency of different Cas nucleases at the indicated target sites. The GFP disruption proportion is referred to as the number of GFP-negative cells relative to the total number of cells. “ng” represents nontargeting guide RNA. “g1” and “g2” indicate site 1 and site 2, respectively ( $N = 3$ , mean  $\pm$  SD from three biological replicates).

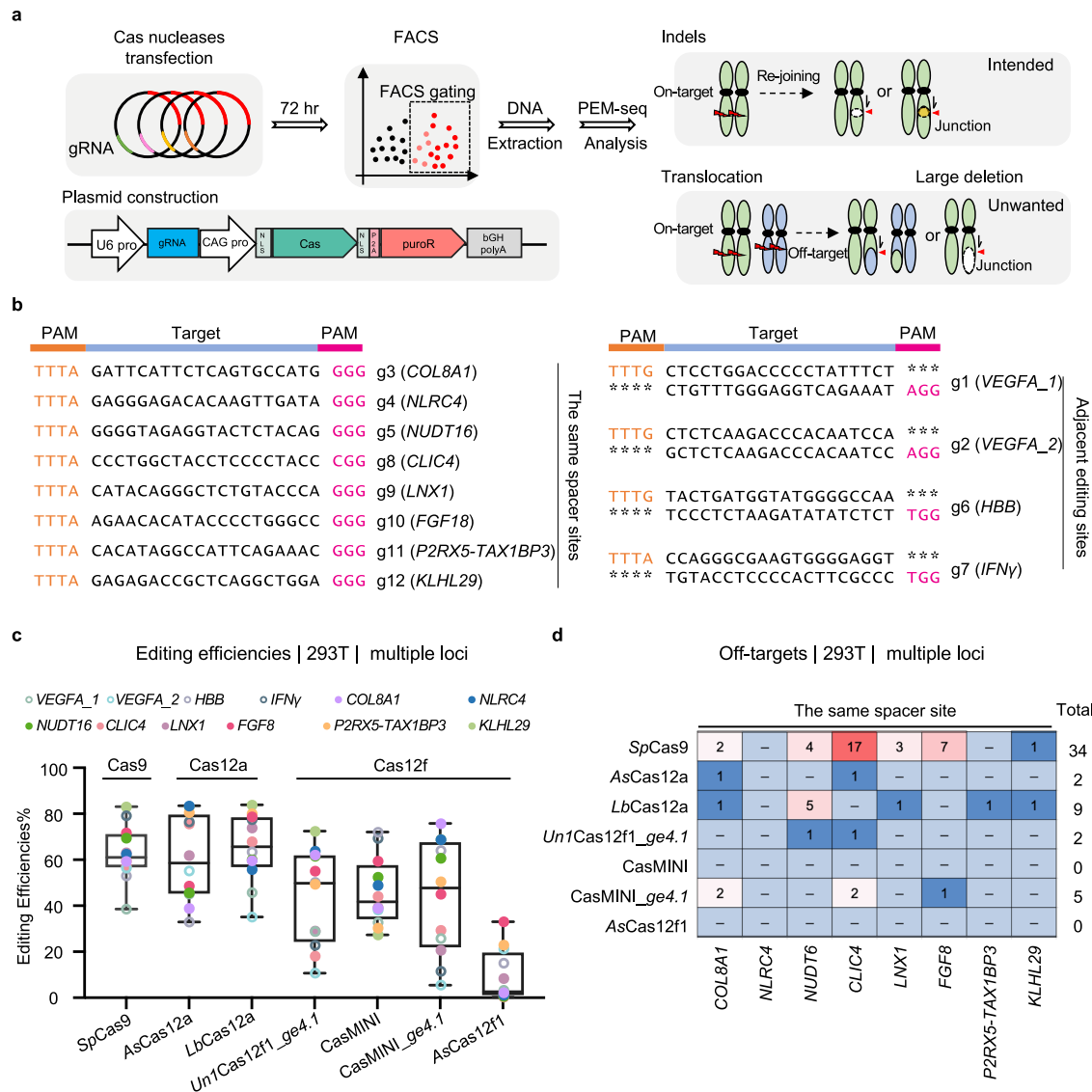


**Fig. 2 | Evaluation of the global editing outcomes of Cas12f nucleases in parallel with Cas9 and Cas12a as determined by PEM-seq.** **a** Schematic diagram showing Cas nuclease evaluation by PEM-seq. The plasmids carrying both Cas nuclease-mCherry and single guide (sg) RNA were transfected into HEK293T cells, and the successfully transfected cells were sorted via FACS 72 h post-transfection followed by PEM-seq construction. PEM-seq can simultaneously detect and quantify small indels, large deletions, and chromosomal translocations with off-targets or general double-strand breaks (DSBs). **b** Detailed guide (g) RNA sequence information of the 12 target sites with PAM sequences for Cas12 and Cas9 in orange or fuchsia, respectively. These target sites were categorized into adjacent editing sites with

different gRNA sequences and same-spacer sites with consistent gRNA sequences. **c** Editing efficiency of the Cas nucleases at the indicated 12 loci as detected by PEM-seq. Editing efficiency indicates the total percentage of insertions, deletions, and translocations. Values from minimum to maximum are shown by the whiskers, and the bounds of the box indicate the first and third quartile ( $N = 12$ ). The vertical line through the box is the median. Source data are provided as a Source Data file. **d** Number of off-target editing at the same-spacer sites as detected by PEM-seq methods and identified through the PEM-Q pipeline. “-” means there was no detected off-target site. The indicated locus and Cas nuclease information are marked.

the second target site (55.1%) and also cleaved the first site with an efficiency of 11.8%. Notably, CasMINI<sub>ge4.1</sub> did not show better activity than CasMINI. Moreover, AsCas12f1 and PlmCas12e showed only slight GFP silencing at both sites (<5.7% and <16.3%, respectively) (Fig. 1d). Recently, an optimized Cas12e variant, PlmCas12e-R1-v2, has been reported to be able to enhance editing efficacy<sup>18</sup>. We found that PlmCas12e-R1-v2 indeed improved editing efficiencies at both target sites than PlmCas12e (46.0% vs. 16.3% and 14.3% vs. 1.8%, respectively) (Fig. 1d and Supplementary Fig. 1b). These results implied that most of the Cas12f nucleases and the optimized Cas12e can be used for gene editing and encouraged us to perform additional experiments to explore the details of their editing activity.

**CRISPR-Cas12f nucleases show high fidelity during gene editing**  
 We next employed a previously developed primer-extension-mediated sequencing (PEM-seq) method to profile the editing outcomes of Cas12f nucleases, assessing both intended small insertions/deletions (indels) and unwanted chromosomal rearrangements such as large deletions, off-target translocations, and general translocations (Fig. 2a)<sup>30,38</sup>. We designed 12 target sites within or adjacent to the human *VEGFA*, *HBB*, *IFN $\gamma$* , *COL8A1*, *NLRC4*, *NUDT16*, *CLIC4*, *LNK1*, *FGF18*, *P2RX5-TAX1BP3*, and *KLHL29* genes and used the nine abovementioned CRISPR-Cas nucleases to target these sites in HEK293T cells. Eight of the 12 target sites had the same spacer sequence with a TTTA PAM for Cas12 and an NGG PAM for Cas9. The other four gRNAs were designed to target adjacent editing sites within a narrow range of locations to

satisfy differences in PAM specificity (Fig. 2b and Supplementary Table 2). The cells were collected by fluorescence-activated cell sorting (FACS) based on mCherry fluorescence 72 h post-transfection. Genomic DNA was then isolated to prepare PEM-seq libraries (Fig. 2a and Supplementary Fig. 2a).

*SpCas9*, *AsCas12a*, and *LbCas12a* showed comparably high levels of editing efficiency, and *UnlCas12f1.ge4.1*, *CasMINI.ge4.1*, and *CasMINI* exhibited robust cleavage at the 12 tested sites (Fig. 2c). In contrast, *AsCas12f1* effectively cleaved only 5 of 12 target sites (Fig. 2c and Supplementary Data 1), in line with the findings of the eGFP-silencing assay. Unexpectedly, *PlmCas12e* showed very limited or even undetectable cleavage at all target sites; despite the optimized *PlmCas12e-R1-v2* improved editing efficacies at some tested sites, only three sites showed editing efficiencies over 5% (Supplementary Fig. 2b and Supplementary Data 1); therefore, we excluded both *PlmCas12e* and *PlmCas12e-R1-v2* from further analyses. In addition to its high-editing ability, *SpCas9* showed robust off-target activity at most of the editing sites, with the number of identified off-target sites being 0 for three sites and 1–17 for the other nine sites (Fig. 2d and Supplementary Fig. 2c and Supplementary Data 2). In contrast, *AsCas12a* and *LbCas12a* showed lower off-target activity, and even fewer off-target sites were identified for the Cas12f family nucleases at both the same spacer sites and adjacent editing sites (Fig. 2d and Supplementary Fig. 2c, d). Notably, no off-target site was identified for *CasMINI* or *AsCas12f1*, although *CasMINI* showed editing efficiency at these tested sites comparable to that of the other CRISPR-Cas enzymes. Collectively, these results indicate that Cas12f family nucleases, especially *CasMINI*, show higher specificity than Cas9 or Cas12a.

### Cas12f nucleases tend to induce small deletions during gene editing

We next sought to investigate repair outcomes during gene targeting by CRISPR-Cas12f. Strikingly, the vast majority of the editing events were deletions by Cas12a and Cas12f, with percentages greater than 92%, from the lowest for *LbCas12a* (92.4%) to the highest for *AsCas12f1* (96.4%), and all were significantly higher than the percentage of deletions induced by *SpCas9* (69.9%) (Fig. 3a)<sup>20,24</sup>. The preponderance of deletions by Cas12a or Cas12f may have been a result of the staggered cleaved DNA ends being processed by endogenous DNA nucleases promoting deletions not insertions. In this context, we found that the Cas12a- or Cas12f-edited products were highly enriched with small deletions (<100 bp) with most small deletions with lengths correlated to the distance between the two staggered cleavage sites of Cas12a or Cas12f (Fig. 3b, c). Specifically, *SpCas9* showed a higher proportion of 1–2-bp deletion fragments, while *AsCas12a*- and *LbCas12a*-edited products were largely 3–7 bp deletion fragments, and the action of the four Cas12f enzymes led to 2–11-bp deletion products, as exemplified by the highly edited *FGF18* target sites (Fig. 3c, Supplementary Figs. 3a and 4a).

We further explored the distribution patterns of deletions induced by these CRISPR-Cas enzymes. The distribution profiles of the Cas12a and Cas12f family enzymes resembled the profile of *SpCas9*, showing similar distribution patterns of gross deletions (Supplementary Fig. 4b). However, compared to *SpCas9*, both Cas12a and Cas12f family enzymes showed higher percentages of deletions from 20- to 60-bp (Fig. 3d and Supplementary Data 3). Notably, the engineered sgRNA *ge4.1* led to an increase in deletion length, as *UnlCas12f1.ge4.1* and *CasMINI.ge4.1* induced more deletions from 20- to 60-bp than *CasMINI* (32.9% and 31.3% vs. 21.3%; Fig. 3d). In addition, all the tested CRISPR-Cas enzymes generated very few deletion fragments of 60 to 100 bp (Fig. 3d). The percentage of deleterious large deletions induced by *SpCas9* was 1.92%. Cas12a generated large deletions to an extent similar to *SpCas9*, with 1.40% and 2.29% large deletions produced by *AsCas12a* and *LbCas12a*, respectively. In contrast, 1.23% and 1.27% of the deletion fragments produced by *UnlCas12f1.ge4.1* and *CasMINI.ge4.1*,

respectively, were large deletions, with and the percentages even smaller, at 0.93% and 0.50%, for *CasMINI* and *AsCas12f1*, respectively (Fig. 3e). Therefore, the Cas12f family nucleases, especially *CasMINI* and *AsCas12f1*, induce only a limited number of large deletions.

### Cas12f nuclease activity leads to fewer integrated vectors than those generated by SpCas9 during genome editing

Compared to those of deletions, the percentages of insertions produced by Cas12a and Cas12f family nucleases were lower, falling to 2.4–5.9% from 26.6% at the 12 target sites for *SpCas9* (Fig. 4a). Consequently, more insertions of all lengths, from 1 bp, 2–25 bp to 25–40 bp and even larger fragments, were observed after *SpCas9* editing (Fig. 4b and Supplementary Data 4). We noticed that the insertions in the *KLHL29*, *COL8A1* and *CLIC4* target loci induced by *SpCas9* were 83.1%, 48.4%, and 43.7%, respectively, higher than the average levels of insertions (Fig. 4a and Supplementary Fig. 5a). These exceptionally frequent insertions were results of 1-bp insertions that were identical to the fourth nt upstream of NGG, which occupied 93.9%, 84.1%, and 78.9% of the total insertion events in *KLHL29*, *COL8A1*, and *CLIC4*, respectively (Supplementary Fig. 5a, b), in line with previous findings<sup>39,40</sup>. In addition to the abovementioned 1-bp insertions, the Cas12a and Cas12f family nucleases produced fewer insertions of 40- and 60-bp and more insertions of 2- and 25-bp, as exemplified by the length distribution at the *HBB* site (Fig. 4c and Supplementary Fig. 5c). The enrichment of insertions in the 2- to 25-bp range due to Cas12a and Cas12f editing might be explained by gaps filled in with generated sticky ends before rejoining (Supplementary Fig. 5d), while the insertions in the 40- to 60-bp might involve vector integration<sup>31</sup>.

Next, we extracted the inserted DNA sequences from PEM-seq libraries and aligned them to the Cas nuclease-expressing vectors at all tested loci and found hundreds to thousands of distinct inserted sequences originating from the transfected vectors. The frequency of vector insertion by *SpCas9* was ~5.2 thousand per 100 thousand on-target indels. The Cas12a and Cas12f family enzymes exhibited a slight decrease in vector integration level, while *CasMINI* and *AsCas12f1* showed a more significant decrease in vector integration (Fig. 4d and Supplementary Table 3). We then mapped the integrated vector fragments across the respective plasmids and found that the inserted vector fragments had been distributed across the plasmid backbone, with accumulation at the AAV inverted terminal repeat region for all the nucleases (Fig. 4e), in line with previous reports<sup>31,41</sup>. In conclusion, the Cas12a and Cas12f family nucleases induce vector integration at a lower rate than *SpCas9*.

### Cas12f induces substantial genomic structural variations

Genomic structural variations, including the abovementioned large deletions and chromosomal translocations, are the most deleterious editing products generated during CRISPR-Cas9 genome editing<sup>32,41</sup>. In this context, we found that ~3.55% of all edits in *SpCas9*-edited cells were chromosomal translocations. The percentages of translocations were reduced to 1.42% and 1.77% for *AsCas12a* and *LbCas12a*, respectively. *UnlCas12f1.ge4.1* and *CasMINI.ge4.1* induced translocations at a level similar to that induced by Cas12a, with percentages of 1.58% and 1.32%, respectively. However, the percentage of translocations induced by either *CasMINI* or *AsCas12f1* was lower, at 1.17% (Fig. 5a, b). Notably, the abundance of translocated fragments was site-specific and varied among different loci (Fig. 5a). In addition, the identified translocations were widely distributed across the whole genome, with obvious enrichment at off-target sites for all the CRISPR-Cas enzymes, as exemplified by the translocations at the *FGF8* target site (Fig. 5b). To comprehensively evaluate the effects of these Cas nucleases, we calculated the editing safety score of these enzymes by combining their off-target activity with the extent of structural variations they induced at effectively edited sites and aligned the score on the basis of the editing efficiency score. The distribution profile of the resulting two-

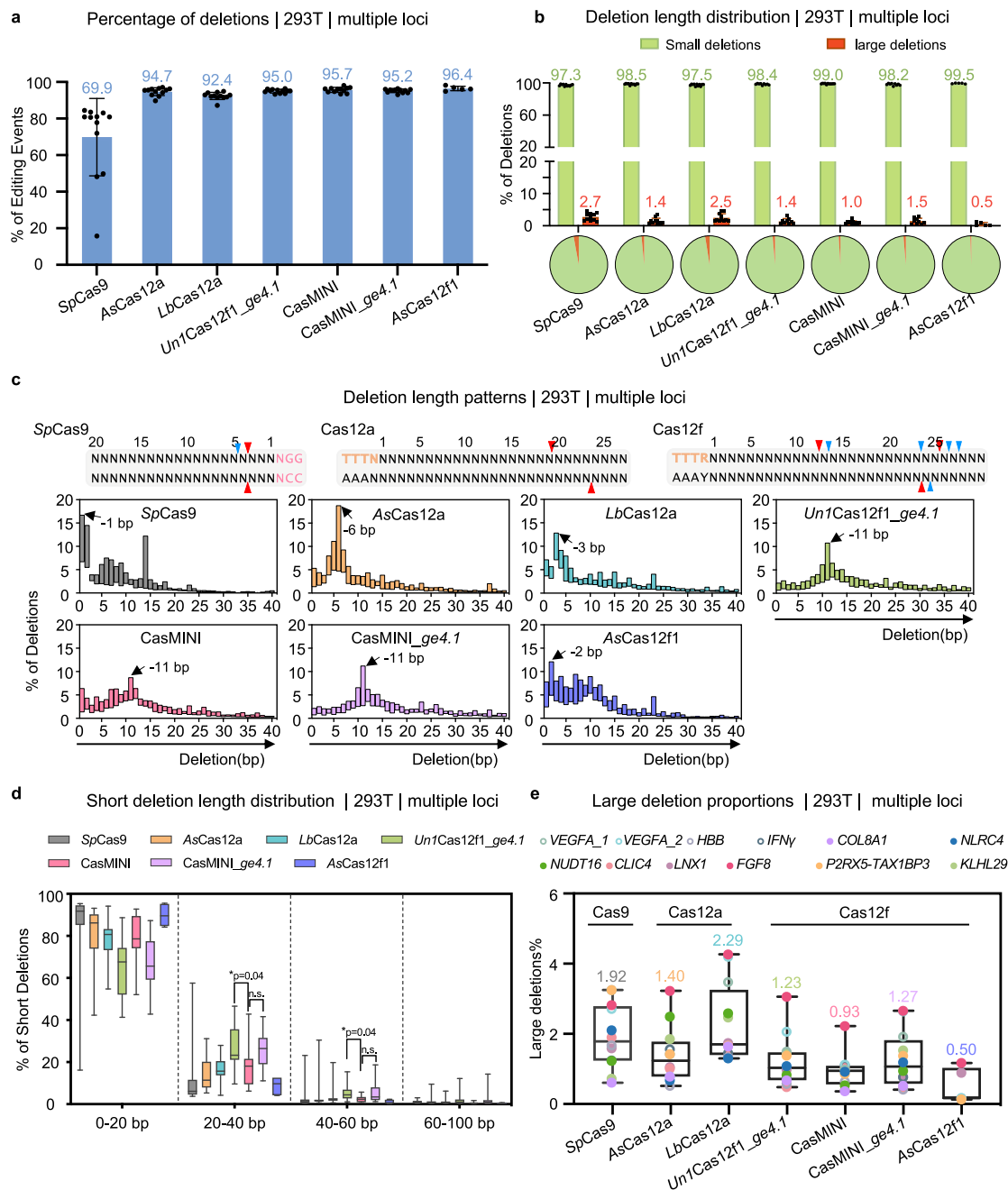
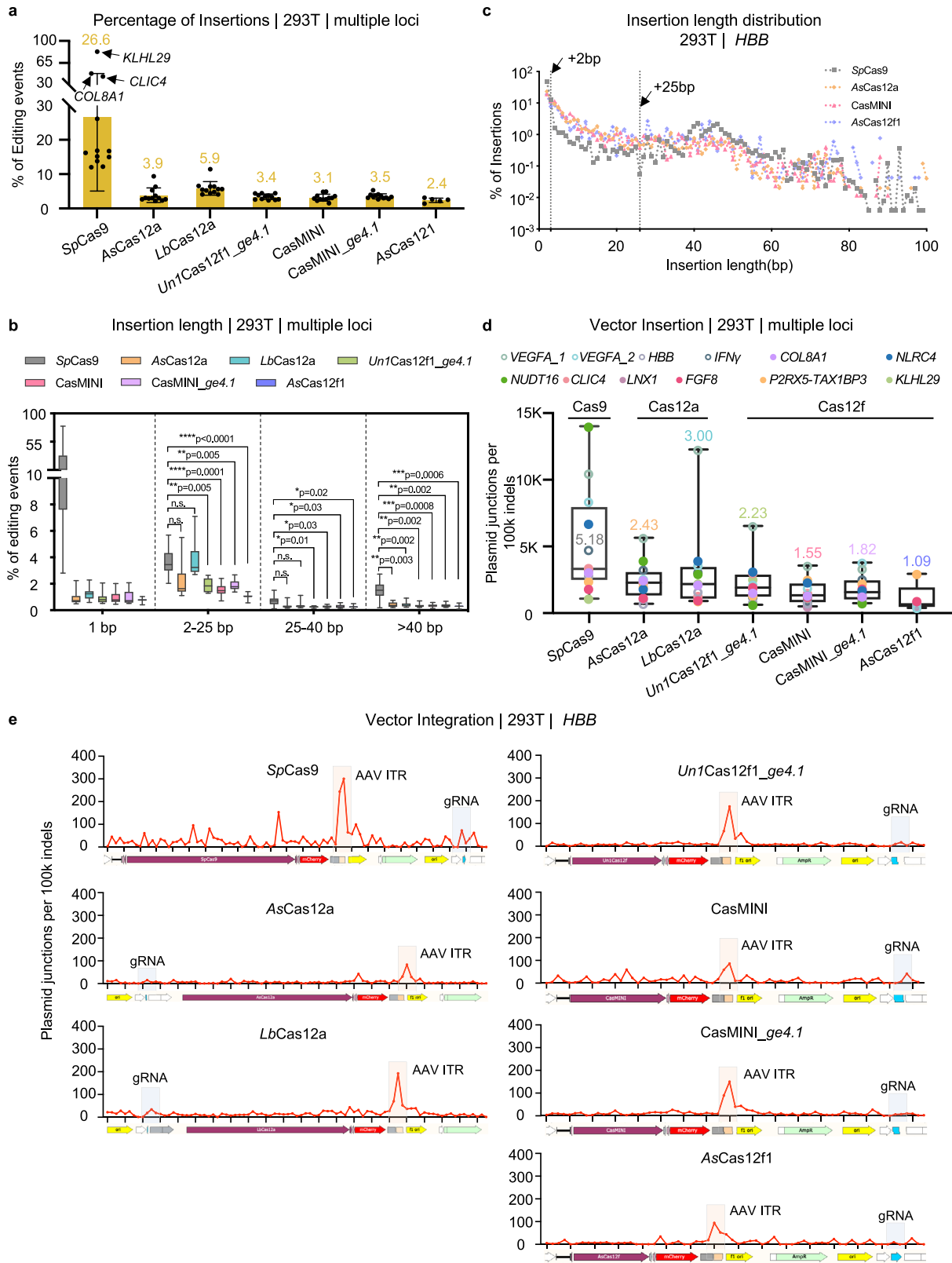


**Fig. 3 | Compared to Cas9, the Cas12a and Cas12f nucleases generated more deletion fragments.** **a** Bar chart showing the percentages of deletions for the indicated Cas nucleases as detected by PEM-seq. The numbers above the bars refer to the average percentages of deletion fragments at all sites for which editing activity was observed (For *SpCas9*, *AsCas12a*, *LbCas12a*, *Un1Cas12f1\_ge4.1*, *CasMINI* and *CasMINI\_ge4.1*,  $n = 12$ ; for *AsCas12f1*,  $n = 5$ ). Data are presented as mean  $\pm$  SD.). **b** Above: bar chart showing the percentages of small deletions ( $\leq 100$  base pairs (bp), in green) and large deletions ( $> 100$  bp, in red) at 12 loci as detected by PEM-seq in HEK293T cells. Bottom: pie chart showing the average percentages of indicated deletions at 12 loci ( $N = 12$ , data are presented as mean  $\pm$  SD. Notably, for *AsCas12f1*,  $n = 5$ ). **c** Above: the double-strand DNA cleavage patterns induced by Cas9, Cas12a, and Cas12f nucleases. Red and blue arrowheads indicate the major and minor cleavage sites, PAM sequences for Cas12 and Cas9 are in orange or fuchsia, respectively. Bottom: size and positional information of the deletions, within a length of 40 bp, generated by the indicated Cas nucleases at all tested sites. The vertical axis indicates the average ratio refers to the number of deletion fragments with the indicated length to the total number of deletion events. The most

abundant deletion size for all tested nucleases is indicated by the black arrow. **d** The distribution of short deletions with the indicated length for all tested nucleases at 12 loci in HEK293T cells. Short deletions were divided into four lengths: 0–20 bp, 20–40 bp, 40–60 bp, and 60–100 bp, and the vertical axis indicates the number of special deletions to total number of short deletions. Values from minimum to maximum are shown by the whiskers, and the bounds of the box indicate the first and third quartile ( $N = 12$ , for *AsCas12f1*,  $n = 5$ ). The vertical line through the box is the median. In both 20–40 bp and 40–60 bp deletions, One-way ANOVA with Geisser-Greenhouse correction analysis was performed for the three data sets: *Un1Cas12f1\_ge4.1*, *CasMINI*, and *CasMINI\_ge4.1*.  $*p < 0.1$ , n.s. not significant. **e** The percentage of large deletions caused by the indicated Cas nucleases on the basis of the total editing events for the indicated 12 loci in HEK293T cells as detected by PEM-seq, with the numbers above the whiskers referring to the average percentages of large deletions at all sites. Values from minimum to maximum are shown by the whiskers, and the bounds of the box indicate the first and third quartile ( $N = 12$ , for *AsCas12f1*,  $n = 5$ ). The vertical line through the box is the median. Source data are provided as a Source Data file.



score map indicated that both CasMINI- and AsCas12f1-editing led to accurate editing with high safety, while CasMINI editing was more efficient than that of AsCas12f1 (Fig. 5c).

### Discussion

Genome editing has been or will be used in therapeutic applications for many genetic disorders<sup>8,42,43</sup>. The accuracy, precision, and especially

safety of genome editing have raised grave concerns for the clinical applications of powerful gene-editing tools, including the CRISPR-Cas system. In fact, from the clinical perspective, the safety and deliverability of editing tools have been a longstanding consideration<sup>37,44</sup>. The miniature CRISPR-Cas12f system, with a minimal protein size, ranging from 400 to 700 aa, was developed to overcome application difficulties due to the payload size of the AAV delivery system<sup>20-24</sup>. In this

**Fig. 4 | Cas12f nucleases suppressed vector integration during gene editing.** **a** Bar chart showing the percentages of insertions for the indicated Cas nucleases as detected by PEM-seq, with the numbers above the bars referring to the average percentages of insertions at all sites for which editing activity was observed (For *SpCas9*, *AsCas12a*, *LbCas12a*, *UnlCas12f1\_ge4.1*, *CasMINI* and *CasMINI\_ge4.1*,  $n = 12$ ; for *AsCas12f1*,  $n = 5$ ). Data are presented as mean  $\pm$  SD). The *KLHL29*, *COL8A1*, and *CLIC4* loci in the *SpCas9* panel are indicated by black arrows. **b** The distribution of insertions with the indicated length for all tested nucleases at 12 loci in HEK293T cells. Insertions were divided into four lengths: 1 base pair (bp), 2–25 bp, 25–40 bp, and >40 bp, and the vertical axis indicates the number of special insertions to the number of total insertions. Values from minimum to maximum are shown by the whiskers, and the bounds of the box indicate the first and third quartile ( $N = 12$ , for *AsCas12f1*,  $n = 5$ ). The vertical line through the box is the median. In 2–25 bp, 25–40 bp, and >40 bp insertions, One-way ANOVA with Geisser-Greenhouse correction analysis was performed for all seven data sets: *SpCas9*, *AsCas12a*, *LbCas12a*, *UnlCas12f1\_ge4.1*, *CasMINI*, *CasMINI\_ge4.1*, and *AsCas12f1*. n.s. not significant, \* $p \leq 0.1$ , \*\* $p \leq 0.01$ ,

\*\*\* $p \leq 0.001$ , \*\*\*\* $p \leq 0.0001$ . **c** The insertion length distribution with the indicated length at the *HBB* locus in HEK293T cells. Total insertion junctions are plotted on the log scale. The different colors indicate different Cas nucleases. Black arrows mark 2-bp insertions and 25-bp insertions. **d** Statistical analysis of vector integration junction numbers per 100k on-target indels for different Cas nucleases at each of the 12 loci, as detected by PEM-seq cloning from the on-target region, with the numbers above the whiskers or within the boxes referring to the average percentages of vector integration numbers at all sites. K means thousand. Values from minimum to maximum are shown by the whiskers, and the bounds of the box indicate the first and third quartile ( $N = 12$ , for *AsCas12f1*,  $n = 5$ ). The vertical line through the box is the median. Source data are provided as a Source Data file. **e** The distribution of vector cleavage and integration junctions across the respective plasmids for every 100k indels for the different Cas nucleases at the *HBB* locus as detected by PEM-seq. K means thousand. Bin size = 100 bp. The adeno-associated virus (AAV) inverted repeat (ITR) region and the guide (g) RNA scaffold are highlighted with pale-yellow and light blue shadows, respectively.

study, we systematically assessed the editing properties of Cas12f nucleases in parallel with the prevalently used Cas9 and Cas12a nucleases. Cas12f showed robust cleavage activity in the mammalian genome but with an efficiency generally lower than that of Cas9 or Cas12a; moreover, *AsCas12f1* showed poor editing outcomes at most target sites (Fig. 2c). *AsCas12f1* is a thermophilic nuclease, and this property might prevent *AsCas12f1* from achieving maximum effectiveness in human cells<sup>24</sup>. Regarding the intended editing products, including mostly indels, compared to Cas9, both Cas12a and Cas12f tended to induce more deletional products, which were correlated with the overhang length generated by the asymmetrical cleavage of two DNA strands by Cas12 enzymes (Fig. 3a, c). In this context, a Cas12-based strategy may be useful for editing the genomes in genetic diseases for which specific DNA fragment deletions are desired<sup>45,46</sup>. Correspondingly, the 1-bp insertions that were abundant among *SpCas9*-edited products and the number of integrated vectors were not typical products of Cas12a or Cas12f editing (Fig. 4b–d and Supplementary Fig. 5a).

Furthermore, the Cas12f nucleases were characterized by relatively higher specificity and safety than Cas9 and Cas12a nucleases. The observed higher specificity of the Cas12f nucleases might be due to the overall lower activity at the on-target sites in comparison to Cas9 and Cas12a nucleases. However, we also noticed that both *CasMINI* and *AsCas12f1* had undetectable off-target effects at the tested sites and generated very few large deletions or translocations in some effectively edited loci (Figs. 2d, 3e, 5a and Supplementary Fig. 2b), which suggested that the long overhangs (~11 bp) of cleaved ends may be also involved in suppressing structural variations by affecting the DNA repair pathways. Conclusively, in cases where the Cas12f enzyme can efficiently induce DNA modifications at target sites, Cas12f nucleases may help maintain genome integrity. In the context of editing ability, *CasMINI* is a relatively better choice than *AsCas12f1*, but the editing efficiency of *CasMINI* needs to be evaluated before use (Fig. 5c). For example, further study with mouse disease models is needed to validate the in vivo properties of *CasMINI*. Finally, further optimization is required to further broaden the target range or improve the editing efficacy of *CasMINI* as well as *AsCas12f1*.

## Methods

### Plasmid construction

Different Cas nucleases were cloned into the same pX330 plasmid vector (Addgene ID 42230) with puromycin resistance gene co-expression with the P2A self-cleavage peptide for 293T-d2EGFP assay or with the mCherry marker gene for cell sorting in the PEM-seq assay. The DNA sequences of different Cas nucleases and gRNA scaffolds were displayed in Supplementary Data 5. The gRNA was cloned into the

same vector with a U6 promoter. All the gRNA sequences are shown in Supplementary Table 2.

### Cell culture and plasmid transfection

HEK293T cells (a gift from Dr. Frederick Alt Lab, Harvard Medical School) were cultured in Dulbecco's modified Eagle's medium (Corning) with 10% Fetal Bovine Serum (ExCell Bio), Penicillin–Streptomycin (Corning), and L-Glutamine (Corning) at 37°C with 5% CO<sub>2</sub>. HEK293T cells cultured in 6-cm dishes were transfected with 6  $\mu$ g of pX330-Cas-nuclease-P2A-mCherry plasmid with 18  $\mu$ l of 1 mg/ml Poly(ethylenimine) (PEI; Sigma). Cas nuclease-transfected cells were harvested 72 h post-transfection with an Aria SORP flow cytometry sorter on the basis of mCherry expression. Then, genomic DNA was extracted for PEM-seq library construction.

### PEM-seq assay and PEM-Q analysis

Each PEM-seq DNA library was constructed according to the standard procedure<sup>30,38</sup>, for which 20  $\mu$ g of genomic DNA from different Cas nuclease-edited samples is generally required. The primer control of each target site was generally applied to the genome of wild-type HEK293T cells transfected by a Cas nuclease without sgRNA targeting. For the PEM-seq procedure, first, the genomic DNA was sonicated with a Covaris M220 Focused Ultrasonicator to obtain 300–700 bp DNA fragments. Then, a biotinylated primer was designed within 150 bp from the target site to accomplish primer extension. Biotinylated single-stranded DNA was enriched with Streptavidin C1 beads and ligated with a “bridge adaptor”, which was designed to achieve exponential amplification of the target fragments. On-bead nested PCR was performed with I5 and I7 primers followed by size selection and amplification with indexed Illumina primers. Then, the DNA libraries were sequenced on an Illumina HiSeq platform by GENEWIZ. The bioprimers and nested primers used in this study are shown in Supplementary Table 2.

A description of the bioinformatics analysis tools and PEM-Q pipeline can be found in the previous study<sup>31</sup>.

### 293T-EGFP cell GFP disruption assay

The 293T-EGFP reporter cell lines were generated by homologous repair-mediated gene knock-in. We used a gene target plasmid to cut the *AAVS1* site and an integration donor plasmid to achieve site-specific exogenous d2EGFP gene insertion. The EF1-alpha promoter was used to drive EGFP gene expression. After transducing 293T cells with the target vector and donor vector, EGFP-positive cells were selected by FACS for subcloning, and d2EGFP gene integration was ensured by PCR. For the procedure of editing efficiency detection in HEK293T-d2EGFP cell lines, plasmids containing a Cas nuclease and a sgRNA that could target EGFP gene sequences were transfected into

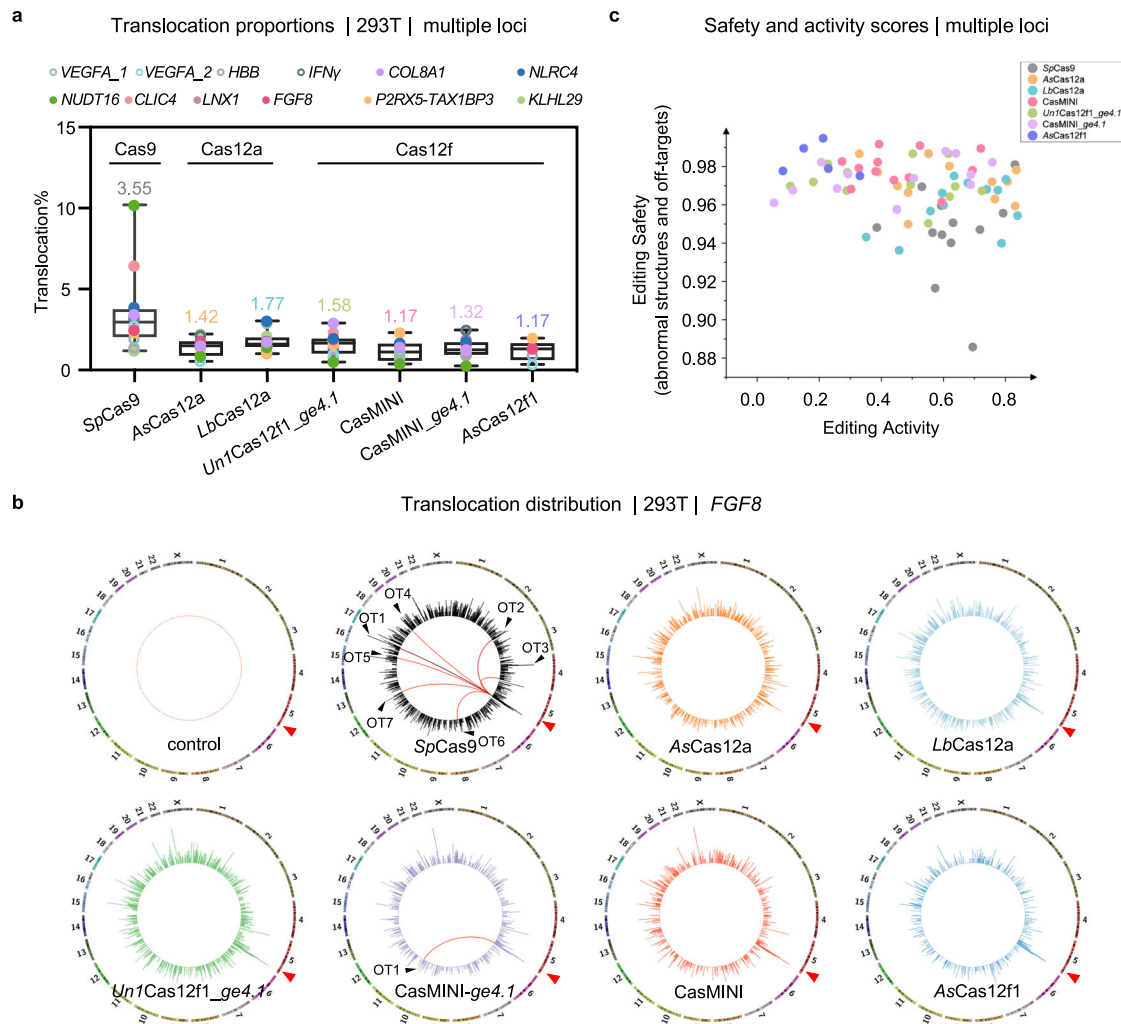


**Fig. 5 | Cas12f nucleases minimized the frequency of chromosomal translocations.** **a** The percentage of translocations caused by the indicated Cas nucleases on the basis of the total editing events for the indicated 12 loci in HEK293T cells as detected by PEM-seq, with the numbers above the whiskers referring to the average percentages of the translocations at all sites. Values from minimum to maximum are shown by the whiskers, and the bounds of the box indicate the first and third quartile ( $N = 12$ , for *AsCas12f1*,  $n = 5$ ). The vertical line through the box is the median. Source data are provided as a Source Data file. **b** The translocation distribution patterns across the whole genome (circos plot) for the indicated Cas nucleases at

the *FGF8* locus in HEK293T cells. The junction signals were binned into 2-Mb intervals and plotted on the log scale. Red and black arrowheads indicate the on-target and off-target cleavage sites, respectively. **c** Activity and safety scores for all tested Cas nucleases at all 12 loci. Of note, we only could calculate the editing safety scores at effectively cleaved sites, so for *SpCas9*, *AsCas12a*, *LbCas12a*, *Un1Cas12f1\_ge4.1*, *CasMINI*, and *CasMINI\_ge4.1*, 12 sites were shown; for *AsCas12f1*, five sites were shown. The activity score was referred to actual editing efficiencies of each point; the safety scores were calculated as  $[1 - (\text{general translocations} \% + \text{off-target junctions} \% + \text{large deletions} \%)]$ .

d2EGFP cells. After the protein was expressed for 1 day, the positively transfected cells were selected with 1.5  $\mu\text{g}/\mu\text{l}$  puromycin for 3 days. The GFP-negative proportion of the cell population was detected by FACS on 5 and 10 days post-transfection and analyzed by FlowJo 10.4 software.

### PEM-Q analysis

Typically, the PEM-Q pipeline can identify several genome editing products: perfect rejoinders, indels, translocations, and other chromosomal abnormalities. The number of indels and translocations to the total number identified products was defined as the editing efficiency ratio. Deletions were defined as small deletions ( $\leq 100$  bp) and large deletions ( $> 100$  bp). Insertions were defined as small insertions ( $< 20$  bp) and large insertions ( $\geq 20$  bp). For off-target analysis, translocation hotspots with sequences very similar to that of the target site ( $\leq 8$  nt mismatches including both the spacer and PAM sequences) and with more than 3 junctions at the presumed cut-site were considered off-target sites. Additionally, translocation junctions within 100 bp of the detected off-target site were regarded as

off-target translocations. General translocations excluded both junctions within 500 kb upstream and downstream of target sites and off-target translocations.

### Statistics and reproducibility

All biological phenomenon studies were developed with at least five sample sizes. Data are presented as the mean  $\pm$  SD, the detailed information about sample sizes can be found in figure legends. One-way ANOVA with Geisser-Greenhouse correction statistical analysis was performed on at least three biologically independent experiments by Graphpad prism8, and  $p < 0.05$  was considered significant. No statistical method was used to predetermine the sample size. No data were excluded from the analyses, the experiments were not randomized, and the investigators were not blinded to allocation during experiments and outcome assessment.

### Reporting summary

Further information on research design is available in the Nature Research Reporting Summary linked to this article.



## Data availability

The Original PEM-seq sequencing data generated in this study have been deposited in both the NCBI Gene Expression Omnibus (GEO) database under accession code [GSE213149](https://www.ncbi.nlm.nih.gov/geo/query/acc.cgi?acc=GSE213149) and the NODE (National Omics Data Encyclopedia) database with accession code [OEP003371](https://www.ncbi.nlm.nih.gov/nodetool/). All plasmids used in this study are available upon request by contacting J.H. ([hujz@pku.edu.cn](mailto:hujz@pku.edu.cn)). Except for unforeseen circumstances, requests will be answered within 1 week. Source data are provided with this paper.

## Code availability

The supported PEM-seq analysis code has been uploaded on the GitHub website: <https://github.com/JiazhiHuLab/PEM-Q>.

## References

- Cong, L. et al. Multiplex genome engineering using CRISPR/Cas systems. *Science* **339**, 819–823 (2013).
- Jinek, M. et al. RNA-programmed genome editing in human cells. *Elife* **2**, e00471 (2013).
- Zetsche, B. et al. Cpf1 is a single RNA-guided endonuclease of a class 2 CRISPR-Cas system. *Cell* **163**, 759–771 (2015).
- Zetsche, B. et al. Multiplex gene editing by CRISPR-Cpf1 using a single crRNA array. *Nat. Biotechnol.* **35**, 31–34 (2017).
- Kim, D. et al. Genome-wide analysis reveals specificities of Cpf1 endonucleases in human cells. *Nat. Biotechnol.* **34**, 863–868 (2016).
- Xu, L. et al. CRISPR-edited stem cells in a patient with HIV and acute lymphocytic leukemia. *N. Engl. J. Med.* **381**, 1240–1247 (2019).
- Cyranoski, D. Chinese scientists to pioneer first human CRISPR trial. *Nature* **535**, 476–477 (2016).
- Frangoul, H. et al. CRISPR-Cas9 gene editing for sickle cell disease and beta-thalassemia. *N. Engl. J. Med.* **384**, 252–260 (2021).
- Gillmore, J. D., Maitland, M. L. & Lebowitz, D. CRISPR-Cas9 in vivo gene editing for transthyretin amyloidosis. *Reply. N. Engl. J. Med.* **385**, 1722–1723 (2021).
- Zhang, Y. et al. CRISPR-Cpf1 correction of muscular dystrophy mutations in human cardiomyocytes and mice. *Sci. Adv.* **3**, e1602814 (2017).
- Zhang, L. et al. AsCas12a ultra nuclease facilitates the rapid generation of therapeutic cell medicines. *Nat. Commun.* **12**, 3908 (2021).
- Yang, Y. et al. A dual AAV system enables the Cas9-mediated correction of a metabolic liver disease in newborn mice. *Nat. Biotechnol.* **34**, 334–338 (2016).
- Zetsche, B., Volz, S. E. & Zhang, F. A split-Cas9 architecture for inducible genome editing and transcription modulation. *Nat. Biotechnol.* **33**, 139–142 (2015).
- Kempton, H. R., Goudy, L. E., Love, K. S. & Qi, L. S. Multiple input sensing and signal integration using a split Cas12a system. *Mol. Cell* **78**, 184–191 (2020).
- Dong, J. Y., Fan, P. D. & Frizzell, R. A. Quantitative analysis of the packaging capacity of recombinant adeno-associated virus. *Hum. Gene Ther.* **7**, 2101–2112 (1996).
- Colella, P., Ronzitti, G. & Mingozzi, F. Emerging issues in AAV-mediated in vivo gene therapy. *Mol. Ther. Methods Clin. Dev.* **8**, 87–104 (2018).
- Liu, J. J. et al. CasX enzymes comprise a distinct family of RNA-guided genome editors. *Nature* **566**, 218–223 (2019).
- Tsuchida, C. A. et al. Chimeric CRISPR-CasX enzymes and guide RNAs for improved genome editing activity. *Mol. Cell* **82**, 1199–1209 (2022).
- Burstein, D. et al. New CRISPR-Cas systems from uncultivated microbes. *Nature* **542**, 237–241 (2017).
- Kim, D. Y. et al. Efficient CRISPR editing with a hypercompact Cas12f1 and engineered guide RNAs delivered by adeno-associated virus. *Nat. Biotechnol.* **40**, 94–102 (2022).
- Harrington, L. B. et al. Programmed DNA destruction by miniature CRISPR-Cas14 enzymes. *Science* **362**, 839–842 (2018).
- Karvelis, T. et al. PAM recognition by miniature CRISPR-Cas12f nucleases triggers programmable double-stranded DNA target cleavage. *Nucleic Acids Res.* **48**, 5016–5023 (2020).
- Xu, X. et al. Engineered miniature CRISPR-Cas system for mammalian genome regulation and editing. *Mol. Cell* **81**, 4333–4345 (2021).
- Wu, Z. et al. Programmed genome editing by a miniature CRISPR-Cas12f nuclease. *Nat. Chem. Biol.* **17**, 1132–1138 (2021).
- Frock, R. L. et al. Genome-wide detection of DNA double-stranded breaks induced by engineered nucleases. *Nat. Biotechnol.* **33**, 179–186 (2015).
- Tsai, S. Q. et al. GUIDE-seq enables genome-wide profiling of off-target cleavage by CRISPR-Cas nucleases. *Nat. Biotechnol.* **33**, 187–197 (2015).
- Cho, S. W. et al. Analysis of off-target effects of CRISPR/Cas-derived RNA-guided endonucleases and nickases. *Genome Res.* **24**, 132–141 (2014).
- Anderson, K. R. et al. CRISPR off-target analysis in genetically engineered rats and mice. *Nat. Methods* **15**, 512–514 (2018).
- Hoffmann, E. R. & Roig, I. Cas9 in human embryos: on target but no repair. *Cell* **183**, 1464–1466 (2020).
- Yin, J. et al. Optimizing genome editing strategy by primer-extension-mediated sequencing. *Cell Disco.* **5**, 18 (2019).
- Liu, M. et al. Global detection of DNA repair outcomes induced by CRISPR-Cas9. *Nucleic Acids Res.* **49**, 8732–8742 (2021).
- Kosicki, M., Tomberg, K. & Bradley, A. Repair of double-strand breaks induced by CRISPR-Cas9 leads to large deletions and complex rearrangements. *Nat. Biotechnol.* **36**, 765–771 (2018).
- Ma, H. et al. Correction of a pathogenic gene mutation in human embryos. *Nature* **548**, 413–419 (2017).
- Hanlon, K. S. et al. High levels of AAV vector integration into CRISPR-induced DNA breaks. *Nat. Commun.* **10**, 4439 (2019).
- Cullot, G. et al. CRISPR-Cas9 genome editing induces megabase-scale chromosomal truncations. *Nat. Commun.* **10**, 1136 (2019).
- Nelson, C. E. et al. Long-term evaluation of AAV-CRISPR genome editing for Duchenne muscular dystrophy. *Nat. Med.* **25**, 427–432 (2019).
- Doudna, J. A. The promise and challenge of therapeutic genome editing. *Nature* **578**, 229–236 (2020).
- Liu, Y. et al. PEM-seq comprehensively quantifies DNA repair outcomes during gene-editing and DSB repair. *STAR Protoc.* **3**, 101088 (2022).
- Shou, J., Li, J., Liu, Y. & Wu, Q. Precise and predictable CRISPR chromosomal rearrangements reveal principles of Cas9-mediated nucleotide insertion. *Mol. Cell* **71**, 498–509 (2018).
- Allen, F. et al. Predicting the mutations generated by repair of Cas9-induced double-strand breaks. *Nat. Biotechnol.* **37**, 64–72 (2019).
- Zhang, W. et al. In-depth assessment of the PAM compatibility and editing activities of Cas9 variants. *Nucleic Acids Res.* **49**, 8785–8795 (2021).
- Park, S. H. & Bao, G. CRISPR/Cas9 gene editing for curing sickle cell disease. *Transfus. Apher. Sci.* **60**, 103060 (2021).
- Long, C. et al. Postnatal genome editing partially restores dystrophin expression in a mouse model of muscular dystrophy. *Science* **351**, 400–403 (2016).
- Lux, C. T. & Scharenberg, A. M. Therapeutic gene editing safety and specificity. *Hematol. Oncol. Clin. North Am.* **31**, 787–795 (2017).
- Amoasii, L. et al. Gene editing restores dystrophin expression in a canine model of Duchenne muscular dystrophy. *Science* **362**, 86–91 (2018).
- Maeder, M. L. et al. Development of a gene-editing approach to restore vision loss in Leber congenital amaurosis type 10. *Nat. Med.* **25**, 229–233 (2019).

## Acknowledgements

We thank Dr. Bo Zhang (Peking University) for her generous gift of the *LbCas12a* plasmid. We also thank the Flow Cytometry Core at National Center for Protein Sciences at Peking University, particularly Yinghua Guo and Liying Du, for technical help. This work was supported by the Ministry of Agriculture and Rural Affairs of China (NK2022010101), the National Key R&D Program of China (2017YFA0506700), NSFC (grant 32122018 and 31771485), Clinical Medicine Plus X-Young Scholars Project (No. PKU2020LCXQ021), PKU-TSU Center for Life Sciences, and SLS-Qidong Innovation Fund.

## Author contributions

C.X., J.Y., and J.H. conceived and designed the research; M.L. developed the analysis pipeline; C.X., J.Y., S.Y., and L.O. performed the experiments; C.X., J.Y., S.Y., and W.Z. analyzed the data; C.X., J.Y., and J.H. wrote the manuscript.

## Competing interests

The authors declare no competing interests.

## Additional information

**Supplementary information** The online version contains supplementary material available at <https://doi.org/10.1038/s41467-022-33346-1>.

**Correspondence** and requests for materials should be addressed to Jiazhi Hu.

**Peer review information** *Nature Communications* thanks the anonymous reviewer(s) for their contribution to the peer review of this work. Peer reviewer reports are available.

**Reprints and permission information** is available at <http://www.nature.com/reprints>

**Publisher's note** Springer Nature remains neutral with regard to jurisdictional claims in published maps and institutional affiliations.

**Open Access** This article is licensed under a Creative Commons Attribution 4.0 International License, which permits use, sharing, adaptation, distribution and reproduction in any medium or format, as long as you give appropriate credit to the original author(s) and the source, provide a link to the Creative Commons license, and indicate if changes were made. The images or other third party material in this article are included in the article's Creative Commons license, unless indicated otherwise in a credit line to the material. If material is not included in the article's Creative Commons license and your intended use is not permitted by statutory regulation or exceeds the permitted use, you will need to obtain permission directly from the copyright holder. To view a copy of this license, visit <http://creativecommons.org/licenses/by/4.0/>.

© The Author(s) 2022